A Power Factor Oriented Railway Power Flow Controller for Power Quality Improvement in Electrical Railway Power System

Sijia Hu, *Member, IEEE,* Bin Xie, Yong Li, *Senior Member, IEEE,* Xiang Gao, Zhiwen Zhang, Longfu Luo, *Member, IEEE,* Olav Krause, *Member, IEEE,* Yijia Cao, *Senior Member, IEEE*

***Abstract*—Focusing on the freight-train dominant electrical railway power system (ERPS) mixed with ac-dc and ac-dc-ac locomotives (its power factor∈[0.70,0.84]), this paper proposes a power factor oriented railway power flow controller (RPFC) for the power quality improvement of ERPS. The comprehensive relationship of the primary power factor, converter capacity, and the two phase load currents are built in this paper. Besides, as the main contribution of this paper, the optimal compensating strategy suited the random fluctuated two phase loads is analyzed and designed based on a real traction substation, for the purposes of satisfying the power quality standard, enhancing RPFC's control flexibility, and decreasing converter's capacity. Finally, both the simulation and the experiment are used to validate the proposed conceive.**

***Index Terms*—Power factor; negative sequence; power quality; power flow controller; electrical railway power system; converter**

I. INTRODUCTION

CONSIDERING the cost-efficiency, the electrical trains are fed by the single phase grid, which are supplied from the three phase to two phase traction transformer in electrical railway power system (ERPS). Due to the random unbalanced two phase loads, amount of negative sequence currents (NSCs) along with the feeder voltage fluctuation in violent are occurred in the utilities and ERPS itself [1], [2]. Besides, though some new generation trains with PWM-based front end rectifier are launched in Chinese railway's rapid developing period, due to the historic reason, many old-fashion phase controlled ac-dc locomotives still act as the main role (*occupied almost* 85% *of the total railroad mileage* [3]), and this status cannot be changed in a short term. Hence, excepting NSC, reactive power or harmonics (including low and high-order components) are also injected into the high-voltage grid [4]; it is particularly serious in the freight-transportation dominant ERPS mixed with ac-dc and ac-dc-ac trains, where the PF∈[0.70,0.84] [5]. The above issues not only imperil grid reliability and security, but also deteriorate the power quality (PQ) of the surrounding customers. It arouses widespread attentions of related industrial sectors and engineers in the worldwide [6]-[8].

As the popular PQ improvement rig, static var compensator (SVC) [9], [10], static synchronous compensator (STATCOM) [11]-[15], active filter [16]-[21], transformer integrated power conditioner [22]-[24], railway power flow controller (RPFC) [5], [25]-[30], and the well-designed train-mounted front end rectifier [31]-[33] are commonly used in ERPS. Considering the comprehensive performance, RPFC is concerned greatly by related departments due to its compatibility – it can, unlike the above rigs, integrate in the secondary side of almost all kinds of traction transformer. By rebalancing the two phase active power, and compensating the reactive power or harmonics in each phase independently, RPFC can deal with almost all the main PQ problems of ERPS. Additionally, the feeder voltage's stability and the capacity utilization ratio of the main transformer can also be enhanced significantly [26] , [30], which are attractive for improving ERPS's transport capacity and cost-efficiency.

However, the high capacity or initial investment slowdown RPFC's industrial application speed. Up to now, few researches have focused on the capacity controlling of RPFC. Benefit from the well-designed LC branches, a novel LC coupled RPFC (LC-RPFC) proposed in [5] can effectively reduce the VA-capacity of its active part, because the dc-link voltage can be reduced about 30%-40% than the conventional RPFC. However, for resent research, the compensating strategy has to be restricted on the "*full compensation model* (FCM)" in the designing process of the LC-branches, i.e., after compensation,

Manuscript received May 5, 2016; revised July 3, 2016 and August 24, 2016; accepted September 2, 2016. This work was supported in part by the National Nature Science Foundation of China under Grant 51477046 and 51377001, and in part by the International Science and Technology Cooperation Program of China under Grant 2015DFR7 0850.

S. Hu, B. Xie, Y. Li, Z. Zhang, L. Luo, and Y. Cao, are with the College of Electrical and Information Engineering, Hunan University, Changsha 410082, China (e-mail: huda_hsj@163.com; xiebin_1215@163.com; yonglichi@gmail.com; hdzzw@126.com; llf@hnu.edu.cn; yjcao@hnu.edu.cn). (*Corresponding author: Yong Li.*)

X. Gao is with the Dongguan Power Supply Bureau, Guangdong Power Grid Company Ltd., Dongguan 523000, China.

O. Krause is with the School of Information Technology and Electrical Engineering, The University of Queensland, Brisbane, QLD 4072, Australia (e-mail: o.krause@uq.edu.au).

This article has been accepted for publication in a future issue of this journal, but has not been fully edited. Content may change prior to final publication. Citation information: DOI 10.1109/TIE.2016.2615265, IEEE Transactions on Industrial Electronics

the primary power factor (PF) equals to 1, and the primary NSC tends to 0, which means LC-RPFC has to bear the largest compensating current [27]. On the other hand, the Chinese national standard [34] indicates that, the consumer can avoid of penalty when the primary PF≥0.9 and the 95% probability value of the primary voltage unbalance ratio $V_{unb}\%\leq 2\%$ [note: $V_{unb}\%=V_-/V_+\times 100\%$; V_- or V_+: fundamental negative or positive sequence voltage (NSV or PSV)]. So, a large amount of capacity is still wasted in the FCM-designed LC-RPFC. Besides, the achievements obtained from LC-RPFC (or RPFC [28]) are only based on the no-popular *single phase* ERPS (occupied less than 1% of the total railroad mileage in China) though it has some advantages; while, few researches focus on the common used *two phase* system, the design of the LC branches in two phase system are much complex than that in the single one is the main obstacle. All the above unsatisfactory aspects should be further improved in the future study.

For maximizing blocking NSC, a new compensating strategy was proposed in [30]. It focuses on the topic of minimizing NSC for a *given* RPFC's capacity, that is to say, it has no help on the capacity determination in the *designing stage* of RPFC. Besides, considering the short circuit capacity S_d of a traction substation is always designed within 500-1500MVA, we found in the practical engineering project that, after a small amount of compensation, the standard of $V_{unb}\%$ can be easily achieved than the requirement of PF, especially for V/v transformer (note: $V_{unb}\%=1.732V_N I_-/S_d$; V_N: primary normal line voltage, I_-: NSC). That is to say, the *reactive power* should be confirmed to be the main compensating target of RPFC in the ac-dc locomotive dominant ERPS with mixed trains, the regulation of NSC, then, degrades into the subordinate one, but cannot be neglected.

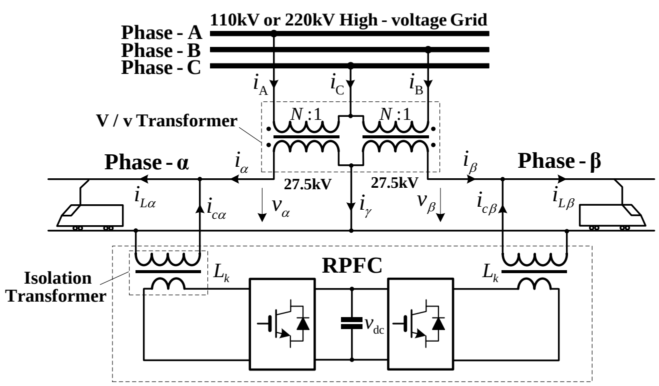

Fig. 1. The typical RPFC integrated two phase ERPS (V/v transformer is adopted as the main transformer).

To further improve RPFC's capacity utilization capability and control flexibility in both designing and operating stages in freight-train dominant ERPS, in this paper, we will focus on the solution of the following aspects:

1) Establishing the relationship between the primary PF with RPFC's compensating capacity; the converter's capacity can be flexibly designed by adjusting the primary PF.
2) In the premise of minimizing RPFC's capacity for a given PF, conceiving an optimal control strategy to decreasing NSC and NSV in a satisfactory level.
3) The proposed control strategy should not only be applied in the simple single phase ERPS, but also in the important common used two phase system (see Fig.1).

This paper is organized as follows, the mathematical model of the RPFC integrated two phase ERPS is presented in Section II. In the premise of mitigation NSC, as the main contribution of this paper, Section III gives the PF oriented optimal compensation strategy for RPFC. Simulation and experiment are given in Section IV and V. Section VI is the conclusion.

II. General Mathematical Model of RPFC Integrated in Two Phase ERPS

First, we define the *frame-ABC* by the V/v transformer's primary three phase voltage $\mathbf{V}_A$, $\mathbf{V}_B$, and $\mathbf{V}_C$, i.e., **Frame-ABC**:

$$\mathbf{V}_A = V_p\angle 0^\circ, \mathbf{V}_B = V_p\angle -120^\circ, \mathbf{V}_C = V_p\angle -240^\circ \tag{1}$$

where V_p is the root mean square (RMS) value of $\mathbf{V}_A$, $\mathbf{V}_B$, and $\mathbf{V}_C$.

Reference to Fig. 1, the phasor diagram of the V/v transformer based ERPS can be obtained, as shown in Fig. 2.

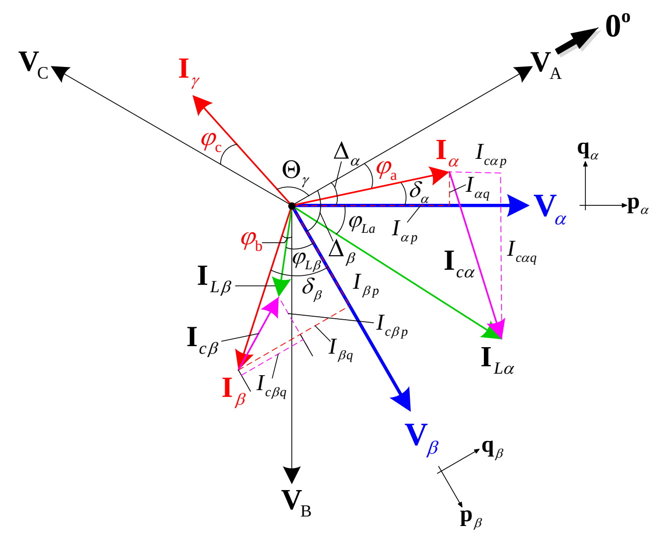

Fig. 2. The phasor diagram of the V/v transformer based ERPC with RPFC.

From Fig. 2, we define the PF in phase-A, B, and C, i.e., PF_A~PF_C as:

$$PF_A = \cos\varphi_a, PF_B = \cos\varphi_b, PF_C = \cos\varphi_c \tag{2}$$

where, $\varphi_k>0$ means that the current lags the voltage, otherwise, the current leads the voltage (k=a, b, c).

It can be seen from Figs. 1 and 2 that, the output currents $\mathbf{I}_\alpha$ and $\mathbf{I}_\beta$ of the V/v transformer in *frame*-$\mathbf{p}_\alpha\mathbf{q}_\alpha$ and *frame*-$\mathbf{p}_\beta\mathbf{q}_\beta$ (see Fig.2) can be expressed as

$$\begin{cases} \mathbf{I}_\alpha = \mathbf{I}_{L\alpha} - \mathbf{I}_{c\alpha} = \underbrace{(I_{L\alpha p} - I_{c\alpha p})}_{I_{\alpha p}} + j\underbrace{(I_{L\alpha q} - I_{c\alpha q})}_{I_{\alpha q}} \\ \mathbf{I}_\beta = \mathbf{I}_{L\beta} - \mathbf{I}_{c\beta} = \underbrace{(I_{L\beta p} - I_{c\beta p})}_{I_{\beta p}} + j\underbrace{(I_{L\beta q} - I_{c\beta q})}_{I_{\beta q}} \end{cases}, \tag{3}$$

where subscript "*p*" and "*q*" represents the active and reactive component of the corresponding variable in *frame*-$\mathbf{p}_\alpha\mathbf{q}_\alpha$ or *frame*-$\mathbf{p}_\beta\mathbf{q}_\beta$, respectively.

Additionally, Fig. 2 also shows that the relationship of the p, q components of $\mathbf{I}_\alpha$ and $\mathbf{I}_\beta$ in frame-$\mathbf{p}_\alpha\mathbf{q}_\alpha$ and $\mathbf{p}_\beta\mathbf{q}_\beta$ satisfy:

This article has been accepted for publication in a future issue of this journal, but has not been fully edited. Content may change prior to final publication. Citation information: DOI 10.1109/TIE.2016.2615265, IEEE Transactions on Industrial Electronics

$$\begin{cases} I_{\alpha q} = I_{\alpha p}\tan\delta_\alpha = (I_{L\alpha p} - I_{c\alpha p})\tan\delta_\alpha \\ I_{\beta q} = I_{\beta p}\tan\delta_\beta = (I_{L\beta p} - I_{c\beta p})\tan\delta_\beta \end{cases}, \tag{4}$$

where $\begin{cases} \delta_\alpha = \Delta_\alpha - \varphi_{\mathrm{a}} \\ \delta_\beta = \Delta_\beta - \varphi_{\mathrm{b}} - 120^\circ \end{cases}$.

Note: for V/v transformer, Δ_α=30 °, Δ_β=90 °[27].

Ignoring the converter's losses, and assuming V_α=V_β, the active power balance of the back-to-back converter can lead the result of:

$$I_{c\alpha p} = -I_{c\beta p}. \tag{5}$$

On the other hand, Fig. 2 indicates that $\mathbf{I}_\gamma$'s phase angle Θ_γ in frame-ABC satisfy

$$\Theta_\gamma = 120^\circ - \varphi_{\mathrm{c}} \text{ or } \tan\Theta_\gamma = \tan(120^\circ - \varphi_{\mathrm{c}}). \tag{6}$$

Based on the Kirchhoff's law, $\mathbf{I}_\alpha$, $\mathbf{I}_\beta$, and $\mathbf{I}_\gamma$ in frame-ABC $\mathbf{I}_\alpha^{\mathrm{ABC}}$, $\mathbf{I}_\beta^{\mathrm{ABC}}$, and $\mathbf{I}_\gamma^{\mathrm{ABC}}$ satisfy

$$-\mathbf{I}_\gamma = -\mathbf{I}_\gamma^{\mathrm{ABC}} = \mathbf{I}_\alpha^{\mathrm{ABC}} + \mathbf{I}_\beta^{\mathrm{ABC}}, \tag{7}$$

where

$$\begin{cases} \mathbf{I}_\alpha^{\mathrm{ABC}} = \mathbf{I}_\alpha \angle -\Delta_\alpha \\ \mathbf{I}_\beta^{\mathrm{ABC}} = \mathbf{I}_\beta \angle -\Delta_\beta \end{cases}. \tag{8}$$

Substituting (3), (4), and (8) into (7), the real and imaginary part of -$\mathbf{I}_\gamma$, Term-I and Term-II, can be calculated as

$$\begin{cases} \text{Term-I} = I_{\alpha p}\cos\Delta_\alpha + I_{\alpha q}\sin\Delta_\alpha + I_{\beta p}\cos\Delta_\beta + I_{\beta q}\sin\Delta_\beta \\ \text{Term-II} = -I_{\alpha p}\sin\Delta_\alpha + I_{\alpha q}\cos\Delta_\alpha - I_{\beta p}\sin\Delta_\beta + I_{\beta q}\cos\Delta_\beta \end{cases} \tag{9}$$

Substituting (9) into (6), and considering the expressions of $I_{\alpha p}$, $I_{\alpha q}$, $I_{\beta p}$, and $I_{\beta q}$ in (3)-(5), the relationship of $I_{c\alpha p}$ with the two phase load active currents $I_{L\alpha p}$ and $I_{L\beta p}$ can be calculated as

$$I_{c\alpha p} = \underbrace{\frac{x_1}{x_1 + x_2}}_{\mu_\alpha} I_{L\alpha p} - \underbrace{\frac{x_2}{x_1 + x_2}}_{\mu_\beta} I_{L\beta p}, \tag{10}$$

where

$$\begin{cases} x_1 = \sin\theta_\alpha - \cos\theta_\alpha \tan\delta_\alpha \\ x_2 = \cos\theta_\beta \tan\delta_\beta - \sin\theta_\beta \end{cases}, \begin{cases} \theta_\alpha = \Delta_\alpha - \varphi_{\mathrm{c}} + 120^\circ \\ \theta_\beta = \Delta_\beta - \varphi_{\mathrm{c}} + 120^\circ \end{cases}.$$

Re-substituting (10) into (3)-(5), the compensating currents of RPFC can be obtained as

$$\begin{cases} I_{c\alpha p} = \mu_\alpha I_{L\alpha p} - \mu_\beta I_{L\beta p} \\ I_{c\beta p} = -\mu_\alpha I_{L\alpha p} + \mu_\beta I_{L\beta p} \\ I_{c\alpha q} = -[\tan\varphi_{L\alpha} + (1-\mu_\alpha)\tan\delta_\alpha] I_{L\alpha p} - \mu_\beta \tan\delta_\alpha I_{L\beta p} \\ I_{c\beta q} = \mu_\alpha \tan\delta_\beta I_{L\alpha p} - [\tan\varphi_{L\beta} + (1+\mu_\beta)\tan\delta_\beta] I_{L\beta p} \end{cases}. \tag{11}$$

Multiplying the feeder voltage V_α or V_β in the two sides of (11), RPFC's compensating power in phase α and β, i.e., $P_{c\alpha}$, $Q_{c\alpha}$ and $P_{c\beta}$, $Q_{c\beta}$, can be calculated as

$$\begin{cases} P_{c\alpha} = \mu_\alpha P_{L\alpha} - \mu_\beta P_{L\beta} \\ P_{c\beta} = -\mu_\alpha P_{L\alpha} + \mu_\beta P_{L\beta} \\ Q_{c\alpha} = -[\tan\varphi_{L\alpha} + (1-\mu_\alpha)\tan\delta_\alpha] P_{L\alpha} - \mu_\beta \tan\delta_\alpha P_{L\beta} \\ Q_{c\beta} = \mu_\alpha \tan\delta_\beta P_{L\alpha} - [\tan\varphi_{L\beta} + (1+\mu_\beta)\tan\delta_\beta] P_{L\beta} \end{cases} \tag{12}$$

where $P_{L\alpha}$ and $P_{L\beta}$ are the load's active power in phase α and β.

It can be seen from (12), because Δ_α, Δ_β can be pre-obtained for a certain type of a transformer (e.g., the V/v transformer and other kind of the balance transformers [35], [36]), μ_α and μ_β are only determined by $\mathrm{PF_A}$~$\mathrm{PF_C}$ or φ_{a}~φ_{c} [see (10) and (2)]. Hence, the active and reactive power of the RPFC can be flexibly adjusted by controlling the primary three phase power factors, if the PFs of the two phase loads are pre-calculated [see $\varphi_{L\alpha}$ and $\varphi_{L\beta}$ in (12)], which will be discussed later on.

III. Compensating Strategy Design

A. The Possible Compensating Scheme

For the consideration of designing convenience and the requirement of PF≥0.9, we let

$$\begin{cases} |\varphi_{\mathrm{a}}| = |\varphi_{\mathrm{b}}| = |\varphi_{\mathrm{c}}| \\ \mathrm{PF}^* = \cos\varphi_{\mathrm{k}} \in [0.9, 1], \ \text{k=a, b, c} \end{cases}, \tag{13}$$

where PF^* is the primary reference power factor.

It can be observed from Fig. 2 that $\mathbf{I}_\alpha$, $\mathbf{I}_\beta$, and $\mathbf{I}_\gamma$ (or $\mathbf{I}_{\mathrm{A}}$, $\mathbf{I}_{\mathrm{B}}$, and $\mathbf{I}_{\mathrm{C}}$) may leads or lags $\mathbf{V}_{\mathrm{A}}$, $\mathbf{V}_{\mathrm{B}}$, and $\mathbf{V}_{\mathrm{C}}$, respectively, which means eight (i.e., $8=2^3$) possible combination models with positive or negative value are existed in φ_{a}, φ_{b}, and φ_{c}. Besides, Fig. 2 also indicates the reactive power of converter-α is larger than the one generated by converter-β (i.e., $I_{c\alpha q}$>$I_{c\beta q}$), to reduce the VA-capacity of converter-α, $\mathbf{I}_\alpha$ has to be restricted lagging than $\mathbf{V}_{\mathrm{A}}$ (i.e., φ_{a}>0), so the above eight possible combination models of φ_{a}~φ_{c} will degenerate into four valuable candidates, which are listed in Table I (i.e., Model-2 to -5).

TABLE I
Compensating Scheme of RPFC*

Compensating model	φ_{a}	φ_{b}	φ_{c}
Model-1 (i.e., FCM)	0	0	0
Model-2	>0	<0	>0
Model-3	>0	<0	<0
Model-4	>0	>0	>0
Model-5	>0	>0	<0

* φ_{k}>0 (or <0) means the inductive (or capacitive) PF (k=a, b, and c).

B. Compensating Capacity Analysis

The VA-capacity S_{RPFC} of the RPFC is:

$$S_{\mathrm{RPFC}} = \underbrace{\sqrt{P_{c\alpha}{}^2 + Q_{c\alpha}{}^2}}_{S_{\text{converter}-\alpha}} + \underbrace{\sqrt{P_{c\beta}{}^2 + Q_{c\beta}{}^2}}_{S_{\text{converter}-\beta}} \tag{14}$$

Substituting (12) into (14), the RPFC's VA-capacity in the five compensating model listed in Table I are shown in Fig. 3 [$P_{L\alpha}$ and $P_{L\beta}$ are the two phase loads' active power, PF^*=0.95, and the two phase loads' PF=0.8 (from a substation's data)].

It can be seen from Fig. 3(a) that, the VA-capacity of RPFC belongs to five different surfaces in Model-1~5 respectively. The maximum S_{RPFC} occurs in the single phase loaded condition, in which Model-1, 2, and 4 correspond to $P_{L\alpha}$≠0, $P_{L\alpha\beta}$=0, while the opposite situation belongs to Model-3 and 5. Additionally, a surface spliced by the surfaces of Model-2, 4, and 5 has the minimum S_{RPFC}. Compared with Model-1, i.e., FCM, the capacity decreasing ratio of this spliced surface is about 30%, which can make the converter have higher system reliability and efficiency. So, it can be selected as the optimal compensating surface. If PF^*=0.95, from Fig. 3(b) the *optimal*

This article has been accepted for publication in a future issue of this journal, but has not been fully edited. Content may change prior to final publication. Citation information: DOI 10.1109/TIE.2016.2615265, IEEE Transactions on Industrial Electronics

compensating strategy (OCS) can be preliminary expressed as

$$\mathbf{OCS}|_{\mathbf{PF}^*=0.95}:\begin{cases}\text{Model-5, } 0\text{MW} \le P_{L\beta} < 0.55P_{L\alpha} \\ \text{Model-4, } 0.55P_{L\alpha} \le P_{L\beta} \le 1.67P_{L\alpha} \\ \text{Model-2, } 1.67P_{L\alpha} < P_{L\beta} \le 8\text{MW}\end{cases}. \tag{15}$$

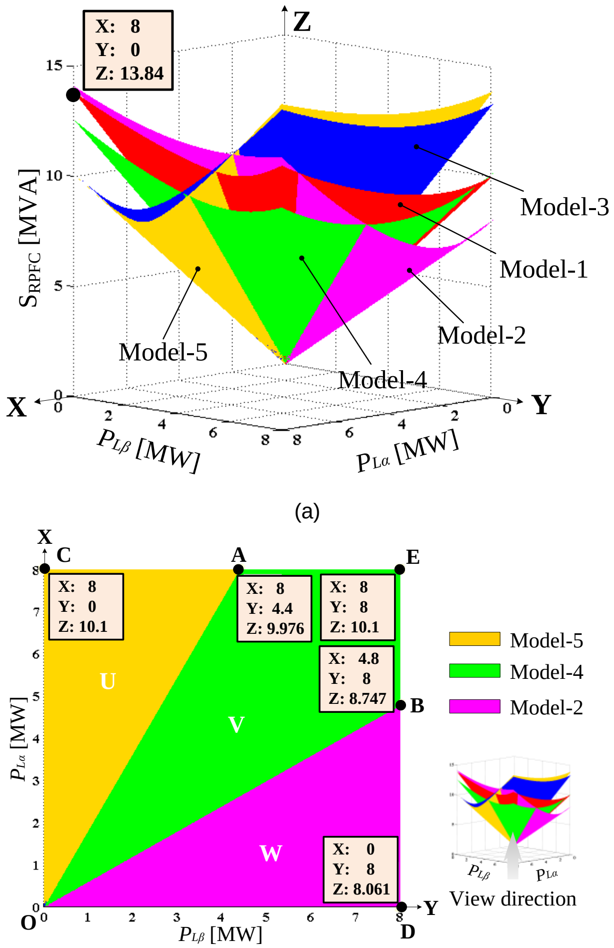

Fig. 3. The relationship of S_{RPFC} with the two phase loads' active power in the five valuable compensating models. (a) The surfaces of SRPFC with the two phase loads' active power. (b) The xoy-projection of the surfaces in Fig. 3(a).

C. The NSC Mitigation Ability Analysis

Excepting of compensating reactive power, mitigation of the NSC is another purpose of RPFC. That is to say, a satisfactory compensating strategy should not only minimize S_{RPFC}, but also has the responsibility to reduce NSC within a satisfactory level.

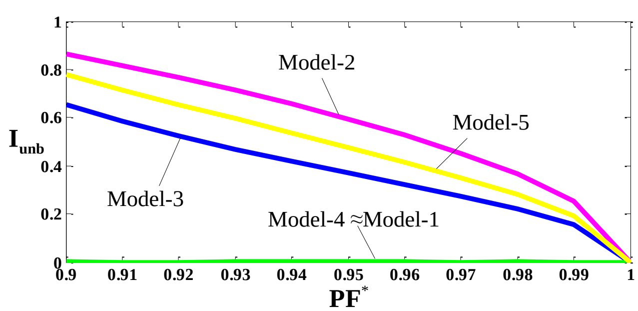

Fig. 4. The curves of I_{unb} v.s. PF^* of Model-1~5.

Combing (7)-(8), the primary positive and negative sequence currents, $\mathbf{I}_+$ and $\mathbf{I}_-$, can be deduced by

$$\begin{aligned}\begin{bmatrix}\mathbf{I}_+\\ \mathbf{I}_-\end{bmatrix} &= \frac{1}{3N}\begin{bmatrix}1 & \xi & \xi^2\\ 1 & \xi^2 & \xi\end{bmatrix}\begin{bmatrix}\mathbf{I}_\alpha^{\text{ABC}}\\ \mathbf{I}_\beta^{\text{ABC}}\\ \mathbf{I}_\gamma^{\text{ABC}}\end{bmatrix}\\ &= \frac{\mu_\beta(I_{L\alpha p}+I_{L\beta p})(1+j\tan\delta_\alpha)}{\sqrt{3}N}\begin{bmatrix}\angle-(\Delta_\alpha-30^\circ)\\ \angle-(\Delta_\alpha+30^\circ)\end{bmatrix}\\ &+\frac{\mu_\alpha(I_{L\alpha p}+I_{L\beta p})(1+j\tan\delta_\beta)}{\sqrt{3}N}\begin{bmatrix}\angle-(\Delta_\beta-90^\circ)\\ \angle-(\Delta_\beta+90^\circ)\end{bmatrix}\end{aligned} \tag{16}$$

where $\xi=\angle 120^\circ$, $N=V_{sN}/V_{fN}$ is the turn's ratio of the main transformer (V_{sN} and V_{fN} are the grid and feeder normal line voltage respectively; as shown in Fig. 1).

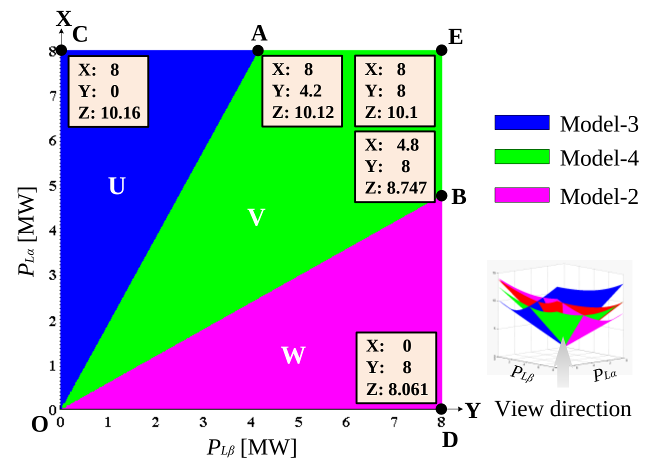

Fig. 5. The optimal compensating strategy of considering the NSC suppressing ability.

From (16), the current unbalance ratio I_{unb} ($I_{unb}=I_-/I_+$) can be obtained as follows.

$$I_{\text{unb}}=\sqrt{\frac{\mu_\alpha^2\cos^2\delta_\alpha+\mu_\beta^2\cos^2\delta_\beta+2\mu_\alpha\mu_\beta\cos\delta_\alpha\cos\delta_\beta\cos(\varphi_a-\varphi_b-180^\circ)}{\mu_\alpha^2\cos^2\delta_\alpha+\mu_\beta^2\cos^2\delta_\beta+2\mu_\alpha\mu_\beta\cos\delta_\alpha\cos\delta_\beta\cos(\varphi_a-\varphi_b-60^\circ)}} \tag{17}$$

From (13), (17), and Table I, the relationship of I_{unb} and PF^* of Model-1~ 5 are shown in Fig. 4. From Fig. 4 and Fig. 3 (a), we can observe that, though the capacity surfaces of Model-3 and 5 are very close [Fig. 3 (a)], the NSC suppressing ability of Model-3 is better than that of Model-5 (Fig. 4). It indicates that, if Model-5 is substituted by Model-3, RPFC can get the better NSC suppressing ability with almost has the same VA-capacity of Model-5. That is to say, the compensating strategy combined of Model-2, 4, and 3 has higher comprehensive performance than the one combined by Model-2, 4, and 5. So the genuine OCS should be modified from Fig. 3(b) into Fig. 5, and its specification is given in (18).

$$\mathbf{OCS}|_{\mathbf{PF}^*=0.95}:\begin{cases}\text{Model-3, } 0\text{MW} \le P_{L\beta} < 0.415P_{L\alpha} \\ \text{Model-4, } 0.55P_{L\alpha} \le P_{L\beta} \le 1.67P_{L\alpha} \\ \text{Model-2, } 1.67P_{L\alpha} < P_{L\beta} \le 8\text{MW}\end{cases} \tag{18}$$

Fig. 6 gives the slopes of line OA and OB, i.e., K_{OA} and K_{OB} in different PF^* (note: OA and OB are the boundaries of the three compensation model shown in Fig. 5; the loads' PF are

This article has been accepted for publication in a future issue of this journal, but has not been fully edited. Content may change prior to final publication. Citation information: DOI 10.1109/TIE.2016.2615265, IEEE Transactions on Industrial Electronics

still confirmed to be 0.8, because the power factor fluctuates in a small rang around 0.8 in the measured substation).

It can be observed from Fig. 6 that, K_{OA}'s fluctuation amplitude is 0.114, while, it varies in relatively large range for K_{OB}. For implementation of the proposed OCS, a satisfactory performance can also be obtained by fixing K_{OA} on 0.5, and adjusting K_{OB} by PF* according the blue curve shown in Fig. 6. It can be pre-embedded in the digital controller's memory space in practical application.

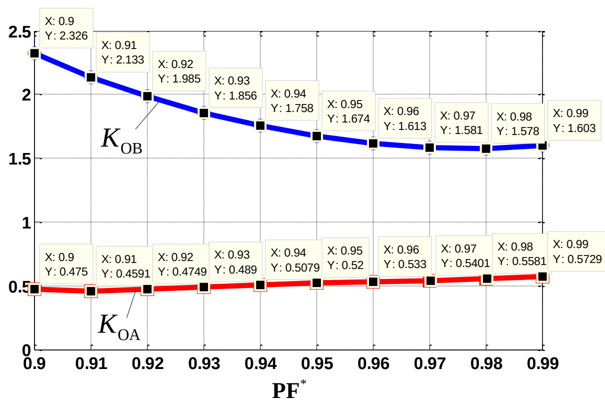

Fig. 6. The curves of slope-AO (i.e., K_{OA}) and BO (i.e., K_{OB}) v.s. PF*.

D. Negative Sequence Standard Consideration

From (16), the primary NSC I_- can be calculated as:

$$I_- = \frac{1}{\sqrt{3}N}\sqrt{\xi_1^2+\xi_2^2}\,(I_{L\alpha p}+I_{L\beta p}), \tag{19}$$

where

$$\begin{cases}\xi_1 = \mu_\alpha[\tan\delta_\beta\cos\Delta_\beta - \sin\Delta_\beta] + \mu_\beta[\cos(\Delta_\alpha+30^\circ)+\tan\delta_\alpha\sin(\Delta_\alpha+30^\circ)] \\ \xi_2 = \mu_\beta[\tan\delta_\alpha\cos(\Delta_\alpha+30^\circ)-\sin(\Delta_\alpha+30^\circ)] - \mu_\alpha[\tan\delta_\beta\sin\Delta_\beta+\cos\Delta_\beta]\end{cases}.$$

The negative sequence capacity S_- in the primary side is

$$S_- = \sqrt{3}V_{sN}I_- = \sqrt{\xi_1^2+\xi_2^2}\,(P_{L\alpha}+P_{L\beta}) = K(P_{L\alpha}+P_{L\beta}). \tag{20}$$

Considering the Chinese national standard of the negative sequence component is

$$\mathrm{V}_{\mathrm{unb}} = \frac{V_-}{V_+} = \frac{S_-}{S_{\mathrm{d}}} \le \varepsilon_V = 2\%, \tag{21}$$

where V_- and V_+ are the primary negative and positive voltages, S_d is the short circuit capacity of the traction substation.

The negative sequence requirement of the proposed system can be calculated by combining (20) and (21), i.e.,

$$K(P_{L\alpha}+P_{L\beta}) \le S_{\mathrm{d}} \times 2\%. \tag{22}$$

Fig. 7 gives the two phase loads' distribution chart of a real V/v transformer based traction substation (see Table II). The statistic results of Fig. 7 indicate that almost 95.2% of the load points are located in the rectangle area of CEDO, where the probability of the points distributed in ΔACO and ΔABO (or ΔAB_1O, or ΔAB_2O) is about 85%. Furthermore, we can also find that, exceeding 50% of the load points are located on the line OC and OD (note: some points are overlapped on these two lines), which means the V/v transformer's capacity utilization ratio can be further improved in a large potential. Based on the above statistic results, our attention should be focused on the loads located in CEDO and its boundaries.

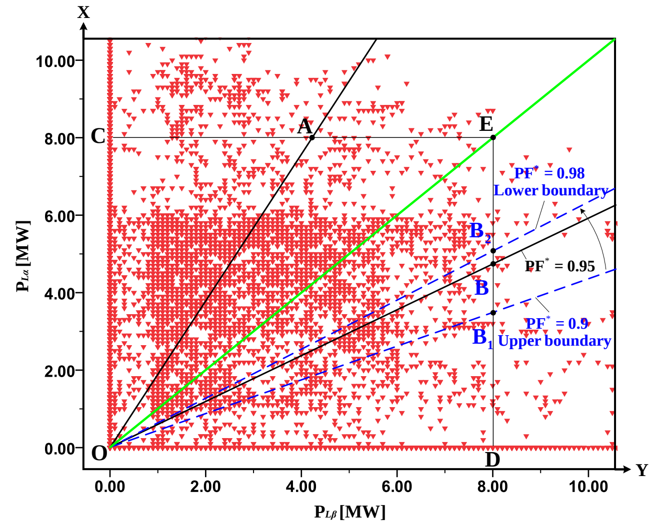

Fig. 7. The two phase load's distribution of a real V/v transformer based traction substation.

TABLE II
THE SPECIFICATION OF A REAL V/V TRANSFORMER

Grid line voltage	110kV
Transformer Capacity	20MVA phase-α: 10MVA phase-β: 10MVA
S_d of the traction substation	486MVA
Short circuit impendence	phase-α and β: 10%
Turn's ratio	110kV:27.5kV

The surface of S_- vs. $P_{L\alpha}$ and $P_{L\beta}$ (within rectangle area of CEDO shown in Fig. 7) can be obtained based on (20) and the S_d given in Table II, which is shown in Fig. 8. From the shape of the surfaces shown in Fig. 8, it can be concluded that the maximum S_- of Model-3, 2, and 4 occurs on the point A, B, and E for any given PF*, respectively.

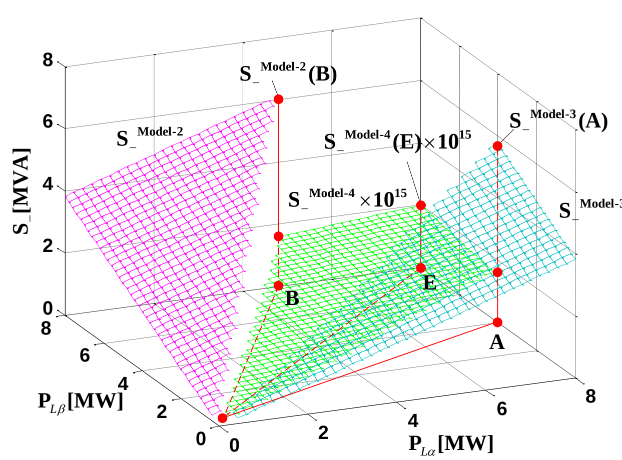

Fig. 8. The relationship of S_- with $P_{L\alpha}$ and $P_{L\beta}$ (note: PF*=0.95).

Fig. 9 gives the relationship of the S_- in A, B, and E, i.e., the maximum S_-, $S_-^{\max}$, with PF* for this traction substation in Model-2~4. Obviously, the S_- blocking capability of Model-4 is much better than that of Model-3 and 2, though the latter's $S_-^{\max}$

This article has been accepted for publication in a future issue of this journal, but has not been fully edited. Content may change prior to final publication. Citation information: DOI 10.1109/TIE.2016.2615265, IEEE Transactions on Industrial Electronics

decreases when PF* becomes large. Fig. 9 also shows that the maximum negative sequence powers controlled by OSC are less than the permission value 9.72MVA (i.e., 486MVA ×2%), which means the Chinese national standard can be satisfied when PF* is set within 0.9 to 0.99. It should be remarked here is that, if the permission line of S_- crosses with other maximum S_- line of Model-2 or 3 shown in Fig. 9, the right hand abscissa of that intersection point should be selected as the valuable PF*, because the left one will lead V_{unb} out of the limit.

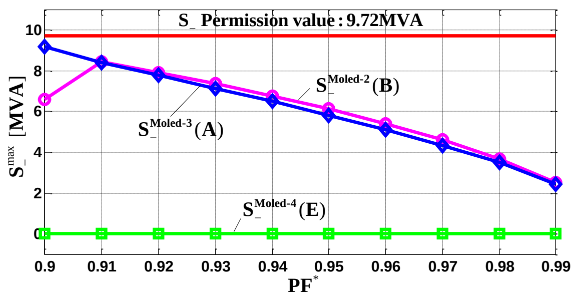

Fig. 9. The relationship of the primary maximum negative capacity with PF* in Modle-2, 3, and 4.

The capacity utilization capability of RPFC should also be included in our concerning scope. From Fig. 10, the maximum S_{RPFC}'s (i.e., $S_{\mathrm{RPFC}}^{\max}$) reducing ratio decreases heavily when PF*>0.95 [note: the maximum S_{RPFC} point in $P_{L\alpha}$-$P_{L\beta}$ panel (i.e., Fig. 7) is labeled in Fig. 10]. Besides, RPFC's designing capacity $S_{\mathrm{RPFC}}^{\mathrm{design}}$'s decreasing ratio also shows relatively large value (>23.43%) when PF*ϵ[0.9,0.95], it increases when PF*→0.9 [note: ① $S_{\mathrm{RPFC}}^{\mathrm{design}}=2\times\max\{S_{\mathrm{conveter}\text{-}\alpha}, S_{\mathrm{conveter}\text{-}\beta}\}$, this is because IGBT is a voltage sensitive device and the dc-link voltages of converter-α and β are the same; ② E_α in Fig.10 means the maximum converter capacity belongs to converter-α located in point E]. Considering cost-efficiency, PF* can be selected from 0.9 to 0.95 for this traction substation.

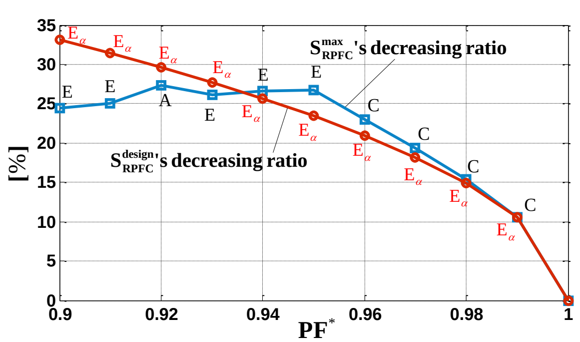

Fig. 10. The relationship of $S_{\mathrm{RPFC}}^{\max}$'s reducing ratio [1-maximum S_{RPFC}/FCM based maximum S_{RPFC}] and $S_{\mathrm{RPFC}}^{\mathrm{design}}$'s reducing ratio [1-$S_{\mathrm{RPFC}}^{\mathrm{design}}$ /FCM based $S_{\mathrm{RPFC}}^{\mathrm{design}}$] with PF* under the control of OCS.

E. Control Strategy Realization

The control system of the RPFC is plotted in Fig. 11. Some specifications should be made for it: The FFT method or the instantaneous reactive power theory [37] can be used for the calculation of the load's active and reactive power in the "PQ block", while the proportional resonant regulator (PS) is adopted as the current controller for its good tracing ability in single phase system. For the stabilization of v_{dc} in the back-to-back system, instead of the calculated $P_{c\alpha}$, the real $P_{c\alpha}$ is generated by the dc-link voltage PI controller in converter-α.

In addition, more attention has to be paid on the realization of the "compensating power calculation" block, and the following four steps can help us to get the target:

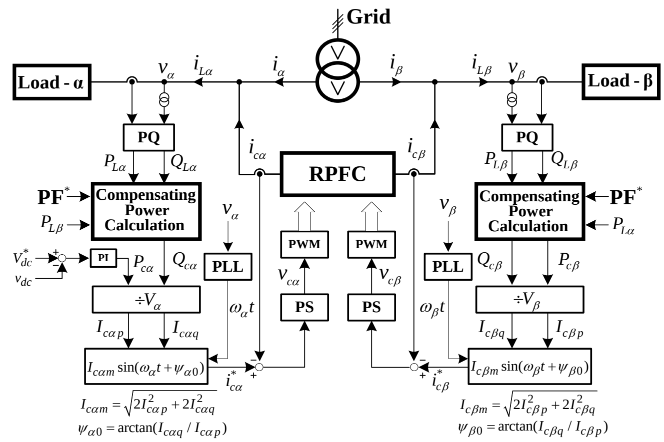

Fig. 11. The control system of the OCS based RPFC.

1) According the measured two phase loads (e.g., Fig. 7), S_{d}, and the presented slops of OA and OB shown in Fig. 6, the PF*'s regulating range can be determined for the purposes of satisfying the negative sequence's standard (e.g., Fig. 9) and having relatively small capacity (e.g., Fig. 10).
2) Based on the pre-set PF* (e.g., PF*ϵ[0.9,0.95]), the slopes of OA and OB can be determined from Fig. 6.
3) The compensating model of OCS can be determined by the load point's location in the load distribution panel shown in Fig. 5 or 7, which can be deduced by detecting the two phase loads' active power $P_{L\alpha}$, $P_{L\beta}$, and the slops of OA and OB pre-obtained in step 2.
4) If the compensating model is obtained from step 3, φ_{a}, φ_{b}, and φ_{c} can be calculated from Table I and (13), so as μ_α and μ_β [see (10)]. Hence, the compensating active and reactive power of RPFC can be finally obtained from (12), [note: in (12), $\varphi_{L\alpha}$=arctan($Q_{L\alpha}/P_{L\alpha}$), $\varphi_{L\beta}$=arctan($Q_{L\beta}/P_{L\beta}$)].

IV. Simulation

To validate the proposed OCS, the simulation model of the studied system shown in Fig. 1 has been established. The parameters of the main transformer, isolation transformer (IT), and converter are listed in Tables II and III.

Fig. 12, Table IV and Fig. 13, Table V are the simulation results in two cases. Fig. 12 corresponds the variable PF* with

TABLE III
The Parameters of The Isolation transformer and RPFC

The VA-capacity of IT	5MVA
Short circuit impendence of IT	21%
IT's turn's ratio [a]	27.5kV:27.5kV
The dc-link voltage of RPFC	51.15kV

[a] For discussion convenience, the turn's ratio of IT is set to be 1:1 in the simulation model, though it is designed to be 27.5kV/1~3kV in the industrial system, where IT has multi-secondary windings and it acts as the interface for the small-rating back-to-back converter unit parallel connection [25]-[26] (note: the multi-level topology is unreliable for RPFC, because of it has the risk of short circuit between the back-to-back converter units [38]).

This article has been accepted for publication in a future issue of this journal, but has not been fully edited. Content may change prior to final publication. Citation information: DOI 10.1109/TIE.2016.2615265, IEEE Transactions on Industrial Electronics

constant load, while the opposite condition belongs to Fig. 13. Figs. 12 and 13 show that, no matter the two phase loads change or not, the primary PF shift along with PF* with the satisfactory performance [Fig. 12(b) and Fig. 13(b)]. Additionally, i_A, i_B, and i_C tend to be the balanced three phase currents when PF* became larger [Fig. 12(a) and Fig. 13(a)], which leads V$_{unb}$%≤2% [Fig. 12(c) and Fig. 13(c)]. Under the governance of OCS, we can also observe from Fig. 12(d) and Fig. 13(d) that S_{RPFC} in all kinds of working conditions are less than that in FCM, e.g., Fig. 12(d), 0.4-0.6s: $S_{RPFC}|_{PF*=0.95}$= 0.72$S_{RPFC}|_{PF*=1}$, Fig. 13(d), 1-1.2s: $S_{RPFC}|_{PF*=0.95}$=0.73$S_{RPFC}|_{PF*=1}$; it is coincident with the theoretical analysis stated in Section III.

TABLE IV
ACTION SEQUENCE OF THE CASE SHOWN IN FIG. 12

Time	PF*	Compensation model	Load condition
0.0-0.2s	No RPFC	-	$P_{L\alpha}$=8MW, $Q_{L\alpha}$=6Mvar; $P_{L\beta}$=0MW, $Q_{L\beta}$=0Mvar
0.2-0.4s	0.90	Model-3	
0.4-0.6s	0.95	Model-3	
0.6-0.8s	0.97	Model-3	
0.8-1.0s	1.00	FCM	

TABLE V
ACTION SEQUENCE OF THE CASE SHOWN IN FIG. 13

Time	Load condition	PF*	Compensation model
0.0-0.2s	$P_{L\alpha}$=0MW, $Q_{L\alpha}$=0Mvar; $P_{L\beta}$=8MW, $Q_{L\beta}$=6Mvar	No RPFC	-
0.2-0.4s	$P_{L\alpha}$=0MW, $Q_{L\alpha}$=0Mvar; $P_{L\beta}$=8MW, $Q_{L\beta}$=6Mvar	1	FCM
0.4-0.6s	$P_{L\alpha}$=8MW, $Q_{L\alpha}$=6Mvar; $P_{L\beta}$=8MW, $Q_{L\beta}$=6Mvar		
0.6-0.8s	$P_{L\alpha}$=8MW, $Q_{L\alpha}$=6Mvar; $P_{L\beta}$=0MW, $Q_{L\beta}$=0Mvar		
0.8-1.0s	$P_{L\alpha}$=0MW, $Q_{L\alpha}$=0Mvar; $P_{L\beta}$=8MW, $Q_{L\beta}$=6Mvar	0.95	Model-2
1.0-1.2s	$P_{L\alpha}$=8MW, $Q_{L\alpha}$=6Mvar; $P_{L\beta}$=8MW, $Q_{L\beta}$=6Mvar		Model-4
1.2-1.4s	$P_{L\alpha}$=8MW, $Q_{L\alpha}$=6Mvar; $P_{L\beta}$=0MW, $Q_{L\beta}$=0Mvar		Model-3

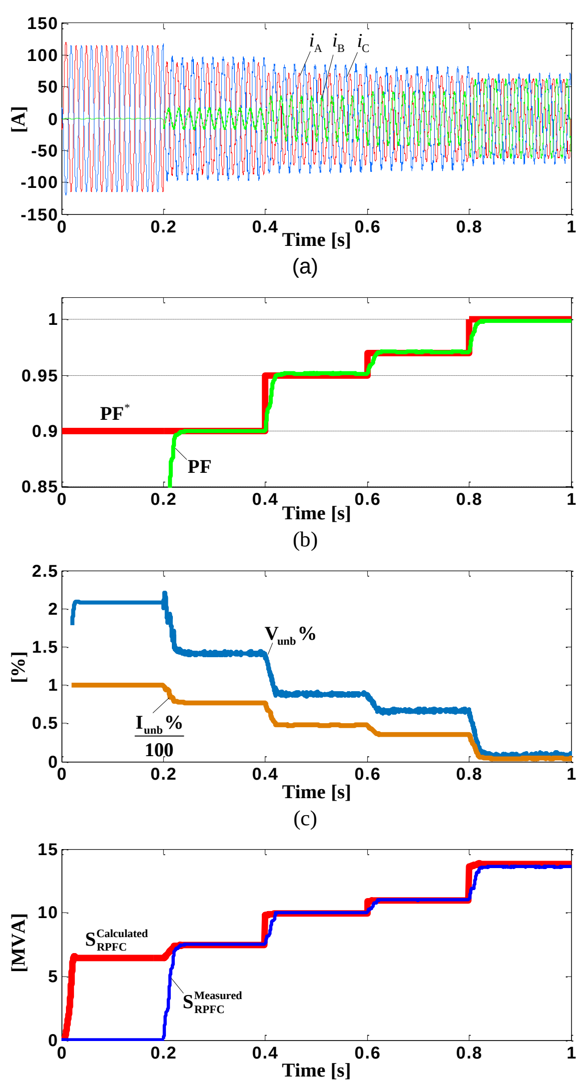

Fig. 12. The waveforms in the condition of variable PF* with constant load. (a) Primary three phase currents. (b) PF* and PF. (c) Voltage's and current's unbalanced ratio. (d) Capacity of RPFC.

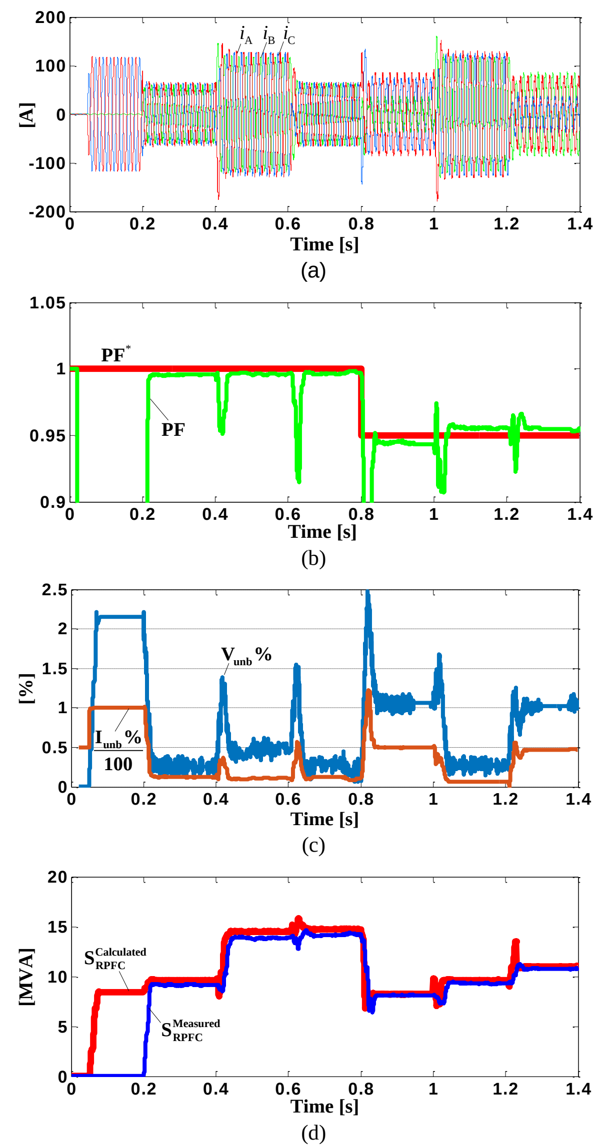

Fig. 13. The waveforms in the condition of variable load with constant PF*. (a) Primary three phase currents. (b) PF* and PF. (c) Voltage's and current's unbalanced ratio. (d) Capacity of RPFC.

This article has been accepted for publication in a future issue of this journal, but has not been fully edited. Content may change prior to final publication. Citation information: DOI 10.1109/TIE.2016.2615265, IEEE Transactions on Industrial Electronics

V. EXPERIMENT

A 2×5kW RPFC was built in laboratory to further validate the proposed strategy. Fig. 14 gives the wiring diagram and the real rig of the experimental system. The OCS is embedded in the main controller (TMS320F2812 DSP), while 1# and 2# slave controller (TMS320 F2812 DSP) are obligated for the regulation of converter-α and -β (sample frequency: 6.4kHz). HIOKI-3198 power quality analyzer is used here for data acquisition. The system parameters are listed Table VI.

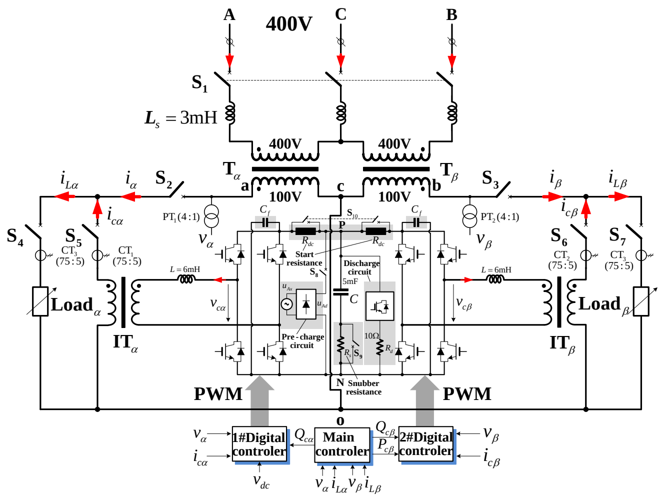

(a)

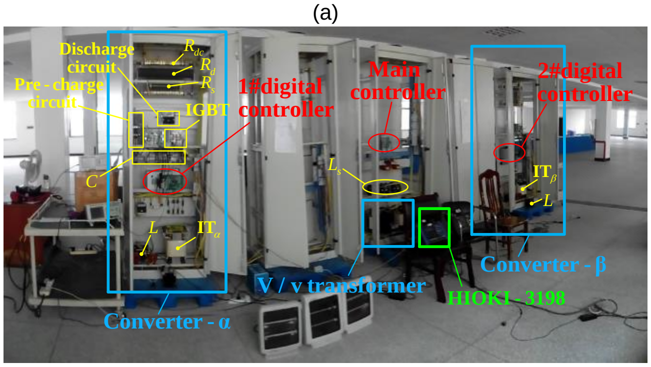

(b)

Fig. 14. Experimental system. (a) Wiring diagram. (b) Real rig.

TABLE VI
THE PARAMETERS OF THE EXPERIMENTAL RPFC

Item	Parameter	Remarks
Grid voltage	400V	–
T_α or T_β	5kVA, 400V:100V	–
IT_α or IT_β	5kVA, 100V:100V	–
L_s	3mH/15A	Enhance the system's inner impedance (the equivalent S_d=73.5kVA)
L	6mH/30A	–
C [a], V_{dc}^*	5mF/400V, 185V	C_f=1.88μF(filtering the dc-link current's high frequency noise) [b]
IGBT	1200V/200 A	Produced by Infineon Technologies AG
Start resistance R_{dc}	1Ω/4kW	Limit IGBT's start current; first switch off S_{10}, and then switch on S_{10}
Snubber resistance R_s	10Ω/200W	In the pre-charge of C, first switch off S_9, and then switch on S_9.
Discharge resistance R_d	10Ω/2kW	When v_{dc}>200V, the discharge circuit starts operation

[a] C is electrolytic capacitor. [b] C_f is non inductance polypropylene capacitor.

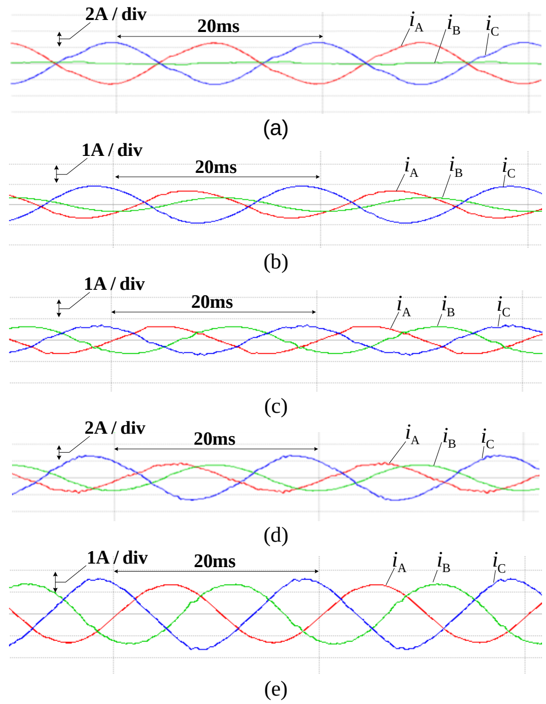

Fig. 15. The waveforms in the condition of variable load with constant PF*. (a) Primary three phase currents. (b) PF* and PF. (c) Voltage's and current's unbalanced ratio. (d) Capacity of RPFC. Experimental waveforms. (a) $P_{L\alpha}$=566W, $Q_{L\alpha}$=424var; $P_{L\beta}$=0W, $Q_{L\beta}$=0var; no RPFC. (b) $P_{L\alpha}$=566W, $Q_{L\alpha}$=424var; $P_{L\beta}$=0W, $Q_{L\beta}$=0var; PF*=0.95. (c) $P_{L\alpha}$=566W, $Q_{L\alpha}$=424var; $P_{L\beta}$=0W, $Q_{L\beta}$=0var; PF*=1. (d) $P_{L\alpha}$=362W, $Q_{L\alpha}$=271var; $P_{L\beta}$=362W, $Q_{L\beta}$=271var; no RPFC. (e) $P_{L\alpha}$=362W, $Q_{L\alpha}$=271var; $P_{L\beta}$=362W, $Q_{L\beta}$=271var; PF*=0.95.

TABLE VII
THE SPECIFICATIONS OF THE EXPERIMENTAL RESULTS

Load condition	PF*	Grid PF	V_{unb}%	I_{unb}%	S_{RPFC}[VA] [a]	
					S_{RPFC}^{cal}	S_{RPFC}^{mea}
$P_{L\alpha}$=566W, $Q_{L\alpha}$=424var; $P_{L\beta}$=0W, $Q_{L\beta}$=0var	No RPFC	0.656	0.974	96.7	0	–
	0.95	0.948	0.362	36.2	719.0	745.3
	1.00	0.995	0.062	3.20	978.8	1015.5
$P_{L\alpha}$=362W, $Q_{L\alpha}$=271var; $P_{L\beta}$=362W, $Q_{L\beta}$=271var	No RPFC	0.701	0.644	49.1	0	–
	0.95	0.941	0.112	5.30	456.9	473.6

[a] S_{RPFC}^{cal}: the calculated S_{RPFC}; S_{RPFC}^{mea}: the measured S_{RPFC}.

Fig. 15 and Table VII give the waveforms and the specifications of the experimental results. In the single phase working condition, as the increase of PF*, i_A, i_B, and i_C tend to be the balanced three phase waveforms [Fig. 15(a)-(c)], the related V_{unb} and I_{unb} are decreased, and the RPFC's capacity is increased, as shown in Table VII. While the similar results are also obtained in two phase working condition [Fig. 15(d)-(e)], except i_A, i_B, and i_C can easier to be made into balance [contrast Fig. 15(b) and (e)]. It is also coincidence with the theoretical analysis aforementioned in Figs. 8 and 9.

VI. CONCLUSION

This paper proposed a power factor oriented RPFC for the power quality improvement in the common used two phase freight train dominated ERPS. The mathematical model of the

RPFC integrated ERPS and the comprehensive design method of the proposed control strategy are given in detail, based on a real traction substation. The simulation and the experimental results verify the correctness of the proposed conceives.

In the premise of satisfying the standards of the reactive power and NSV, this paper gives an optimal control strategy for the PQ improvement, control flexibility enhancement, and the reduction of RPFC's compensating and designing capacity in two or single phase RPFC integrated ERPS. That is to say, this control method can make the system have an attractive high cost-efficiency in two or single phase traction load conditions.

REFERENCES

[1] S. Chen, R. Li, and H.4 Hsiang, "Traction system unbalance problem-analysis methodologies," *IEEE Trans. Power Del*., vol. 19, no. 4, pp. 1877–1883, Oct. 2004.

[2] J. Kilter, T. Sarnet, and T. Kangro, "Modelling of high-speed electrical railway system for transmission network voltage quality analysis: Rail Baltic case study," in *Proc. Elect. Power Qual. Supply Reliab. Conf. (PQ)*, 2014, pp. 323–328.

[3] Z. He, H. Hu, Y. Zhang, and S. Gao, "Harmonic resonance assessment to traction power-supply system considering train model in China high-speed railway," *IEEE Trans. Power Del*., vol. 29, no. 4, pp. 1735–1743, Aug. 2014.

[4] G. Raimondo, P. Ladoux, A. Lowinsky, H. Caron, and P. Marino, "Reactive power compensation in railways based on AC boost choppers," *IET Electr. Syst. Transp.*, vol. 2, no. 4, pp. 169–177, Jua. 2012.

[5] Z. Zhang, Y. Li, L. Luo, P. Luo, Y. Cao, Y. Chen *et al*, "A new railway power flow control system coupled with asymmetric double LC branches," *IEEE Trans. Power Electron*., vol. 30, no. 10, pp. 5484–5498, Oct. 2015.

[6] S. Gazafrudi, A. Langerudy, E. Fuchs, and K. Al-Haddad, "Power quality issues in railway electrification: a comprehensive perspective," *IEEE IEEE Trans. Ind. Electron.*, vol. 62, no. 5, pp. 3081–3090, May. 2015.

[7] T. Uzuka, "Faster than a speeding Bullet: An overview of Japanese high-speed rail technology and electrification," *IEEE Electrification Mag.*, vol.1, no.1, pp. 11–20, Sep. 2013.

[8] M. Brenna, F. Foiadelli, and D. Zaninelli, "Electromagnetic model of high speed railway lines for power quality studies," *IEEE Trans. Power Syst.*, vol. 25, no. 3, pp. 1301–1308, Aug. 2010.

[9] H. Wang, Y. Liu, K. Yan, Y. Fu, and C. Zhang, "Analysis of static VAr compensators installed in different positions in electric railways," *IET Elect. Syst. Transp.*, vol. 5, no. 3, pp. 129–134, Jan. 2015.

[10] G. Zhu, J. Chen, and X. Liu, "Compensation for the negative-sequence currents of electric railway based on SVC," in *Proc. ICIEA. Conf.*, 2008, pp. 1958–1963.

[11] K. Fujii, K. Kunomura, K. Yoshida, A. Suzuki, S. Konishi, M. Daiguji *et al*., "STATCOM applying flat-packaged IGBTs connected in series," *IEEE Trans. Power Electron.*, vol. 20, no. 5, pp. 1125–1132, Sep. 2005.

[12] R. Grunbaum, J. Hasler, T. Larsson, and M. Meslay, "STATCOM to enhance power quality and security of rail traction supply," in *Proc. 8th Int. Symp. Adv. Electro-Mech. Motion Syst. Electr. Drives*, Lille, France, 2009, pp. 1–6.

[13] A. Bueno, J. Aller; J. Restrepo, R. Harley, T. Habetler, "Harmonic and unbalance compensation based on direct power control for electric railway systems," *IEEE Trans. Power Electron.*, vol.28, no.12, pp. 5823-5831, Dec. 2013.

[14] B. Gultekin, C. Gercek, T. Atalik, M. Deniz, N. Bicer, M. Ermis *et al*., "Design and implementation of a 154-kV ±50-Mvar transmission STATCOM based on 21-level cascaded multilevel converter," *IEEE Trans. Ind. Appl.*, vol. 48, no. 3, pp. 1030–1045, May. 2012.

[15] P. Ladoux, G. Raimondo, H. Caron, and P. Marino, "Chopper-controlled steinmetz circuit for voltage balancing in railway substations," *IEEE Trans. Power Electron.*, vol. 28, no. 12, pp. 5813–5882, Dec. 2013.

[16] S. Senini and P. Wolfs, "Hybrid active filter for harmonically unbalanced three phase three wire railway traction loads," *IEEE Trans. Power Electron*, vol. 15, no. 4, pp. 702–710, Jul. 2000.

[17] S. Rahmani, A. Hamadi, K. Al-Haddad, and A. Dessaint, "A combination of shunt hybrid power filter and thyristor controlled reactor for power quality," *IEEE Trans. Ind. Electron.*, vol. 61, no. 5, pp. 2152–2164, May. 2014.

[18] H. Akagi and K. Isozaki, "A hybrid active filter for a three-phase 12-pulse diode rectifier used as the front end of a medium-voltage motor drive," *IEEE Trans. Power Electron.*, vol. 27, no. 1, pp. 69–77, Jan. 2012.

[19] A. Bhattacharya, C. Chakraborty, and S. Bhattacharya, "Parallel connected shunt hybrid active power filters operating at different switching frequencies for improved performance," *IEEE Trans. Ind. Electron.*, vol. 59, no. 11, pp. 4007–4019, Nov. 2012.

[20] P. Tan, P. Loh, and D. Holmes, "Optimal impedance termination of 25-kV electrified railway systems for improved power quality," *IEEE Trans. Power Del*., vol. 20, no. 2, pp. 1703–1710, Apr. 2005.

[21] P. Tan, P. Loh, and D. Holmes, "A robust multilevel hybrid compensation system for 25-kV electrified railway applications," *IEEE Trans. Power Electron.*, vol. 19, no. 4, pp. 1043–1052, Jul. 2004.

[22] S. Hu, Z. Zhang, Y. Li, L. Luo, Y. Cao, and C. Rehtanz, "A new half-bridge winding compensation based power conditioning system for electric railway with LQRI," *IEEE Trans. Power Electron*., vol. 29, no. 10, pp. 5242–5256, Oct. 2014.

[23] S. Hu, Z. Zhang, Y. Chen, G. Zhou, Y. Li, L. Luo *et al*., "A new integrated hybrid power quality control system for electrical railway," *IEEE Trans. Ind. Electron.*, vol. 62, no. 10, pp. 6222–6232, Oct. 2015.

[24] S. Hu, Y. Li, B. Xie, M. Chen, Z. Zhang, L. Luo *et al*., "A y-d multifunction balance transformer-based power quality control system for single-phase power supply system," *IEEE Trans. Ind. Appl*., vol. 52, no. 2, pp. 1270–1279, Mar. 2016.

[25] T. Uzuka, S. Ikedo, K. Ueda, Y. Mochinaga, S. Funahashi, and K. Ide, "Voltage fluctuation compensator for shinkansen," *Trans. IEE Japan*, vol. 162, no. 4, pp. 25–34, May. 2008.

[26] M. Ohmi, and Y. Yoshii, "Validation of railway static power conditioner in Tohoku Shinkansen on actual operation," in *Proc. Int. Conf. Power Electron*., 2010, pp. 2160–2164.

[27] A. Luo, F. Ma, C. Wu, S. Ding, Z, Shuai, and Q. Zhong, "A dual-loop control strategy of railway static power regulator under V/V electric traction system," *IEEE Trans. Power Electron*., vol. 26, no. 7, pp. 2079–2091, Jul. 2011.

[28] N. Dai, M. Wong, K. Lao, and C. Wong, "Modelling and control of a railway power conditioner in co-phase traction power system under partial compensation," *IET Power Electron.*, vol. 7, no. 5, pp. 1044–1054, May. 2014.

[29] F. Ma, Q. Xu, Z. He, C. Tu, Z. Shuai, A. Luo *et al*., "A railway traction power conditioner using modular multilevel converter and its control strategy for high-speed railway system," *IEEE Trans. Transp. Electrif.*, vol. 2, no. 1, pp. 96–109, Mar. 2016.

[30] D. Zhang, Z. Zhang, W. Wang, and Y. Yang, "Negative sequence current optimizing control based on railway static power conditioner in V/v traction power supply system," *IEEE Trans. Power Electron*., vol. 31, no. 1, pp. 2079–2091, Jan. 2016.

[31] B. Bahrani, and A. Rufer, "Optimization-based voltage support in traction networks using active line-side converters," *IEEE Trans. Power Electron*., vol. 28, no. 2, pp. 673–685, Feb. 2013.

[32] C. Zhao, D. Dujic, A. Mester, J. Steinke, M. Weiss, S. Schmid *et al*., "Power electronic traction transformer—medium voltage prototype," *IEEE Trans. Ind. Electron.*, vol. 61, no. 7, pp. 3257–3269, Jul. 2014.

[33] D. Dujic, C. Zhao, A. Mester, J. Steinke, M. Weiss, S. Schmid *et al*., "Power electronic traction transformer—low voltage prototype," *IEEE Trans. Power Electron.*, vol. 28, no. 12, pp. 5522–5534, Dec. 2013.

[34] *Quality of Electric Energy Supply Admissible Three Phase Voltage Unbalance*, National Standard GB/T 15543-2008, 2008.

[35] T. Kneschke, "Control of utility system unbalance caused by single-phase electric traction," *IEEE Trans. Ind. Appl.*, vol. IA-21, no. 6, pp. 1559–1570, Nov. 1985.

[36] F. Ciccarelli, M. Fantauzzi, D. Lauria, and R. Rizzo, "Special transformers arrangement for ac railway systems," in *Proc. Electrical Systems for Aircraft, Railway and Ship Propulsion (ESARS)*, 2012, pp. 1–6.

[37] H. Akagi, E. Watanabe, and M. Aredes, *Instantaneous power theory and applications to power conditioning*. New Jersey, USA: IEEE Press, 2007.

[38] M. Miranbeigi, H. Iman-Eini, and M. Asoodar, "A new switching strategy for transformer-less back-to-back cascaded H-bridge multilevel converter," *IET Power Electron.*, vol. 7, no. 7, pp. 1868–1877, Jan. 2014.

Sijia Hu (S'14-M'16) was born in Hunan, China, in 1987. He received the B.Sc. and Ph.D. degrees in electrical engineering (and automation) from Hunan University of Science and Technology (HNUST), Xiangtan, China, and Hunan University (HNU), Changsha, China, in 2010 and 2015, respectively.

Since 2016, he is an Assistant Professor of Electrical Engineering with HNU. His research interests include power flow and power quality control of electric railway power systems, new topology converters, and stability and power quality analyses and control of multi-converter systems.

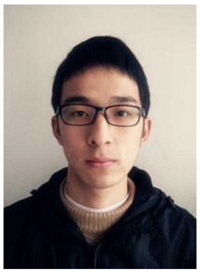

Bin Xie was born in Hunan, China, in 1990. He received the B.Sc. degree in electrical engineering from Shaoyang University in 2013. He is currently working toward the Ph.D. degree of electrical engineering in the College of Electrical and Information Engineering, Hunan University, Changsha, China.

His research interests include power quality analysis and control of electric railway power system, new topology power flow controller.

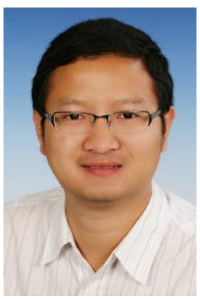

Yong Li (S'09–M'12–SM'14) was born in Henan, China, in 1982. He received the B.Sc. and Ph.D. degrees in 2004 and 2011, respectively, from the College of Electrical and Information Engineering, Hunan University, Changsha, China.

Since 2009, he worked as a Research Associate at the Institute of Energy Systems, Energy Efficiency, and Energy Economics (ie^3), TU Dortmund University, Dortmund, Germany, where he received the second Ph. D. degree in June 2012. After then, he was a Research Fellow with The University of Queensland, Brisbane, Australia. Since 2014, he is a Full Professor of electrical engineering with Hunan University. His current research interests include power system stability analysis and control, ac/dc energy conversion systems and equipment, analysis and control of power quality, and HVDC and FACTS technologies.

Dr. Li is a member of the Association for Electrical, Electronic and Information Technologies (VDE) in Germany.

Xiang Gao was born in Hunan, China, in 1990. He received the B.Sc. and M.Sc. degrees in electrical engineering from Hunan Institute of Engineering and Hunan University in 2013 and 2016 respectively. He is currently working with Dongguan Power Supply Bureau, Guangdong Power Grid Company Ltd., Dongguan, China.

His research interests include power quality analysis and control of electric railway power system, power system protection.

Zhiwen Zhang was born in Hunan, China, in 1963. He received the B.Sc. and M.Sc. degrees in electrical engineering and Ph.D. degree in control theory and control engineering from Hunan University, China, in 1987, 1990, and 2006, respectively.

From 1992 to 1993 and 2006 to 2007, he was a visiting scholar at Tsinghua University, Beijing, China and a Visiting Professor at Ryerson University, Toronto, Canada, respectively. He is currently a Full Professor in the College of Electrical and Information Engineering, Hunan University, Changsha, China. His research interests include power quality analysis and control of electric railway power system, theory and new technology of ac/dc energy transform, theory and application of new-type electric apparatus, harmonic suppression for electric railway, power electronics application, and computer control.

Longfu Luo (M'09) was born in Hunan, China, in 1962. He received the B.Sc., M.Sc., and Ph.D. degrees from the College of Electrical and Information Engineering, Hunan University, Changsha, China, in 1983, 1991, and 2001, respectively.

From 2001 to 2002, he was a Senior Visiting Scholar at the University of Regina, Regina, SK, Canada. Currently, he is a Full Professor of electrical engineering at the College of Electrical and Information Engineering, Hunan University. His current research interests include the design and optimization of modern electrical equipment, the development of new converter transformer, and the study of corresponding new HVDC theories.

Olav Krause (M'05) was born in Germany in 1978. He received the Dipl.-Ing. (ME.) and Dr.-Ing. (Ph.D.) degrees in electrical engineering from the TU Dortmund University, Dortmund, Germany, in 2005 and 2009, respectively.

Currently, he is a Lecturer of Electrical Engineering in the School of Information Technology and Electrical Engineering, The University of Queensland, Brisbane, Australia. His main research interests include distribution network automation, with a focus on state estimation under measurement deficiency and power system load ability determination. This is complemented by work on techniques of probabilistic and harmonic power-flow analysis.

Yijia Cao (M'98-SM'13) was born in Hunan, China, in 1969. He received the Graduation degree from Xi'an Jiaotong University, Xi'an, China, in 1988, and received the M.Sc. and Ph.D. degrees from Huazhong University of Science and Technology (HUST), Wuhan, China, in 1991 and 1994, respectively.

From September 1994 to April 2000, he worked as a Visiting Research Fellow and Research Fellow at Loughborough University, Liverpool University, and University of the West England, U.K. From 2000 to 2001, he was a Full Professor of HUST, and from 2001 to 2008, he was a Full Professor of Zhejiang University, China. He was appointed as a Deputy Dean of College of Electrical Engineering, Zhejiang University, in 2005. Currently, he is a Full Professor and the Vice President of Hunan University, Changsha, China. His research interests include power system stability control and the application of intelligent systems in power systems.